Killer cell immunoglobulin-like receptor 3DL1 polymorphism defines distinct hierarchies of HLA class I recognition

Philippa M. Saunders,[1]* Phillip Pymm,[2,3,4]* Gabriella Pietra,[5,6] Victoria A. Hughes,[2,3,4] Corinne Hitchen,[2] Geraldine M. O'Connor,[1] Fabrizio Loiacono,[7] Jacqueline Widjaja,[1] David A. Price,[8,9] Michela Falco,[7] Maria Cristina Mingari,[5,6] Lorenzo Moretta,[10] Daniel W. McVicar,[11] Jamie Rossjohn,[2,3,4,8]** Andrew G. Brooks,[1]** and Julian P. Vivian[2,3,4]**

[1]Department of Microbiology and Immunology, Peter Doherty Institute for Infection and Immunity, The University of Melbourne, Parkville, Victoria 3010, Australia
[2]Infection and Immunity Program, Biomedicine Discovery Institute, [3]Department of Biochemistry and Molecular Biology, and [4]Australian Research Council Centre of Excellence in Advanced Molecular Imaging, Monash University, Clayton, Victoria 3800, Australia
[5]Department of Experimental Medicine, University of Genova, 16132 Genoa, Italy
[6]IRCCS AOU San Martino-IST (National Institute for Cancer Research), 16132 Genoa, Italy
[7]IRCCS Istituto Giannina Gaslini, 16148 Genoa, Italy
[8]Institute of Infection and Immunity, Cardiff University School of Medicine, Heath Park, Cardiff CF14 4XN, Wales, UK
[9]Human Immunology Section, Vaccine Research Center, National Institute of Allergy and Infectious Diseases, National Institutes of Health, Bethesda, MD 20892
[10]IRCCS Ospedale Pediatrico Bambino Gesù, 00146 Rome, Italy
[11]Cancer and Inflammation Program, National Cancer Institute–Frederick, Frederick, MD 21701

Natural killer (NK) cells play a key role in immunity, but how HLA class I (HLA-I) and killer cell immunoglobulin-like receptor 3DL1 (KIR3DL1) polymorphism impacts disease outcome remains unclear. KIR3DL1 (*001/*005/*015) tetramers were screened for reactivity against a panel of HLA-I molecules. This revealed different and distinct hierarchies of specificity for each KIR3DL1 allotype, with KIR3DL1*005 recognizing the widest array of HLA-I ligands. These differences were further reflected in functional studies using NK clones expressing these specific KIR3DL1 allotypes. Unexpectedly, the Ile/Thr80 dimorphism in the Bw4-motif did not categorically define strong/weak KIR3DL1 recognition. Although the KIR3DL1*001, *005, and *015 polymorphisms are remote from the KIR3DL1–HLA-I interface, the structures of these three KIR3DL1–HLA-I complexes showed that the broader HLA-I specificity of KIR3DL1*005 correlated with an altered KIR3DL1*005 interdomain positioning and increased mobility within its ligand-binding site. Collectively, we provide a generic framework for understanding the impact of KIR3DL1 polymorphism on the recognition of HLA-I allomorphs.

Natural killer (NK) cells play a key innate role in the elimination of infected or transformed cells that are no longer identified as self (Ljunggren and Kärre, 1990). The interaction of inhibitory killer cell immunoglobulin-like receptors (KIRs) with HLA class I (HLA-I) molecules is important during NK cell development and regulates NK cell lysis of target cells that have down-regulated HLA-I expression or express different HLA-I allotypes. The highly polymorphic nature of both KIR and HLA-I has resulted in several studies linking the presence of particular KIR/HLA-I combinations with disease outcomes, in particular in the context of chronic viral infections. For example, the presence of *KIR3DL1* and certain *HLA-I* alleles has been associated with delayed progression to AIDS in HIV-infected individuals (Martin et al., 2007). Nevertheless, the mechanistic basis for such associations remains unclear.

KIR3DL1 recognizes HLA-I allotypes that bear the Bw4 motif, a region that spans residues 77–83 on the α1-helix of the HLA-I molecule. The crystal structure of the KIR3DL1*001–peptide–HLA-B*57:01 complex demonstrated that KIR3DL1 bound two regions that are highly conserved across HLA-I allotypes in addition to residues within the Bw4 motif. Here, the interaction is ultimately dependent on the microarchitecture of the Bw4 motif and the sequence of the bound peptide (Gumperz et al., 1995, 1997; Thananchai et al., 2007; Vivian et al., 2011; O'Connor et al., 2014; Saunders et al., 2015). Additionally, there is evidence that polymorphism both within and outside the Bw4 motif can impact KIR3DL1 recognition (Gumperz et al., 1997; Thananchai et al., 2007; Sanjanwala et al., 2008; O'Connor et al., 2014). For instance, HLA-A*32:01, HLA-B*51:01, and HLA-B*58:01 generally confer robust

*P.M. Saunders and P. Pymm contributed equally to this paper.

**J. Rossjohn, A.G. Brooks, and J.P. Vivian contributed equally to this paper.

Correspondence to Jamie Rossjohn: jamie.rossjohn@monash.edu; Andrew G. Brooks: agbrooks@unimelb.edu.au; or Julian P. Vivian: julian.vivian@monash.edu

Abbreviations used: AML, acute myeloid leukemia; KIR, killer cell immunoglobulin-like receptor; MFI, mean fluorescence intensity.

The Rockefeller University Press $30.00
J. Exp. Med. 2016 Vol. 213 No. 5 791–807
www.jem.org/cgi/doi/10.1084/jem.20152023

protection of target cells from lysis by KIR3DL1$^+$ NK cells, whereas HLA-B*15:13 and HLA-B*27:05 have sometimes been associated with moderate or weak inhibitory effects, despite the fact that all of these molecules are HLA-Bw4 allotypes (Cella et al., 1994; Litwin et al., 1994; Gumperz et al., 1995; Luque et al., 1996; Rojo et al., 1997; Carr et al., 2005; O'Connor et al., 2007; Norman et al., 2009).

Our understanding of the hierarchical HLA-Bw4 preferences of KIR3DL1 is further confounded by polymorphism within the *KIR3DL1* locus. More than 100 allelic variants of the *KIR3DL1* gene have been described, phylogenetically spanning three main lineages based on the sequence differences across the three extracellular domains (D0–D1–D2) of the KIR3DL1 molecule (Norman et al., 2009; Robinson et al., 2015). Namely, there are two diverse inhibitory lineages comprising *KIR3DL1*005*-like and **015*-like alleles, whereas the third lineage is much more constrained at a population level and consists largely of the activating *KIR3DS1*013* allele (Norman et al., 2007; Parham et al., 2012). *KIR3DL1* polymorphism was initially associated with differences in cell surface expression, with allotypes such as KIR3DL1*001, *002, and *008 being expressed at high levels, *005 and *009 at lower levels, and *004 being largely retained intracellularly (Gardiner et al., 2001; Pando et al., 2003; Taner et al., 2011; Mulrooney et al., 2015). *KIR3DL1* polymorphism can also affect recognition of HLA-I with polymorphisms at positions including 238 and 283 impacting recognition of various HLA-Bw4 ligands (Carr et al., 2005; Yawata et al., 2006; Thananchai et al., 2007; O'Connor et al., 2014). Similarly, recent evidence has shown enhanced recognition of HLA-B*44:03 by KIR3DL1*005 relative to KIR3DL1*001 and KIR3DL1*009 (Mulrooney et al., 2015). However, the molecular mechanisms underpinning these effects remain unclear.

Early studies correlated a subset of HLA-Bw4 allotypes possessing Ile at position 80 with elevated protection from lysis by NK cells, which led to the hypothesis that Ile80 marked "high affinity" ligands for KIR3DL1 and even KIR3DS1 (Cella et al., 1994; Martin et al., 2007). This concept has been used to frame subsequent studies examining disease progression. For example, in HIV-infected individuals, the presence of KIR3DL1 allotypes with high cell surface expression in combination with Ile80-encoding HLA-Bw4 allotypes was associated with reduced viral replication and delayed progression to AIDS (Martin et al., 2007). Similarly, the presence of both KIR3DL1 and HLA-Bw4 allotypes with Ile80 was associated with an increased risk of relapse after autologous hematopoietic stem cell transplant for acute myeloid leukemia (AML) relative to patients who lacked Bw4 allotypes or who possessed Bw4 allotypes with Thr80 (Marra et al., 2015). Although these genetic associations are broadly consistent with data showing that position 80 impacts recognition of HLA-Bw4 by KIR3DL1, it remains unclear whether Ile80 is predictive of high-affinity interactions with KIR3DL1. Similarly, the impact of *KIR3DL1* polymorphism on disease outcome is ill defined. Accordingly, to characterize the spectrum of recognition and the functional consequences of given KIR3DL1 and HLA-Bw4 allotypic pairings, the interactions of a range of HLA-I molecules with representatives of the two inhibitory lineages of KIR3DL1, *005 and *015, together with a common interlineage recombinant, KIR3DL1*001, were compared. Using both KIR3DL1 tetramers and functional assays, Ile80 within the Bw4 motif was observed not to define a high-affinity ligand for KIR3DL1. Instead, distinct hierarchies were detected for each KIR3DL1 allotype that assist in reconciling the influence of both KIR3DL1 allotype and HLA-Bw4 polymorphism in determining effective inhibitory capacity. From the ternary crystal structures of KIR3DL1*001, *005, and *015, we show that the dimorphism at position 283 alters the configuration of D1–D2, leading to increased flexibility in KIR3DL1*005, which confers a distinct but broader specificity for HLA-Bw4 allotypes. Our data provide a molecular framework to interpret the impact of KIR3DL1 polymorphism on HLA-I recognition and can be used to inform disease association studies.

RESULTS

KIR3DL1$^+$ NK cells differentiate between HLA-Bw4 molecules

Although numerous studies have shown that KIR3DL1 interactions with HLA-Bw4 allotypes inhibit NK cell activation, the extent to which this varies between individuals and different HLA-I allotypes has remained unclear (Cella et al., 1994; Gumperz et al., 1995, 1997). To address this issue, KIR3DL1$^+$ NK cells obtained from several healthy donors were expanded with IL-2 and then incubated either with 721.221 (221) cells, which lack endogenous HLA-A, -B, and -C, or 221 cells transfected with a range of HLA-I molecules: HLA-B*57:01, -B*58:01, and -A*24:02, which all encode an identical Bw4 motif (NLRIALR), HLA-B*27:05 and HLA-B*44:05, which encode distinct Bw4 motifs containing a Thr at position 80, and HLA-B*08:01, a control allotype that possesses the Bw6 motif (Fig. 1, A and B). The up-regulation of CD107a, a marker for degranulation, was assessed by flow cytometry and normalized against the maximal response to the parental 221 cell line (Fig. 1, C and D).

HLA-B*44:05, HLA-B*57:01, and HLA-B*58:01 efficiently inhibited KIR3DL1$^+$ NK cells, whereas HLA-A*24:02 and HLA-B*27:05 were more limited in this regard, often showing comparable levels of activation with those observed with target cells expressing HLA-B*08:01 (Fig. 1, C and D). These inhibitory effects were not caused by CD94-NKG2A recognition of HLA-E on the cell surface because all assays were performed in the presence of a CD94-blocking antibody (Pende et al., 2009). In line with this, the pattern of inhibition of was not consistent with a CD94-NKG2A/HLA-E–dependent mechanism as HLA-B*08:01– and HLA-A*24:02–derived leader sequence peptides (residues 3–11) form more potent CD94-NKG2A ligands when complexed with HLA-E than those derived from other Bw4 allotypes

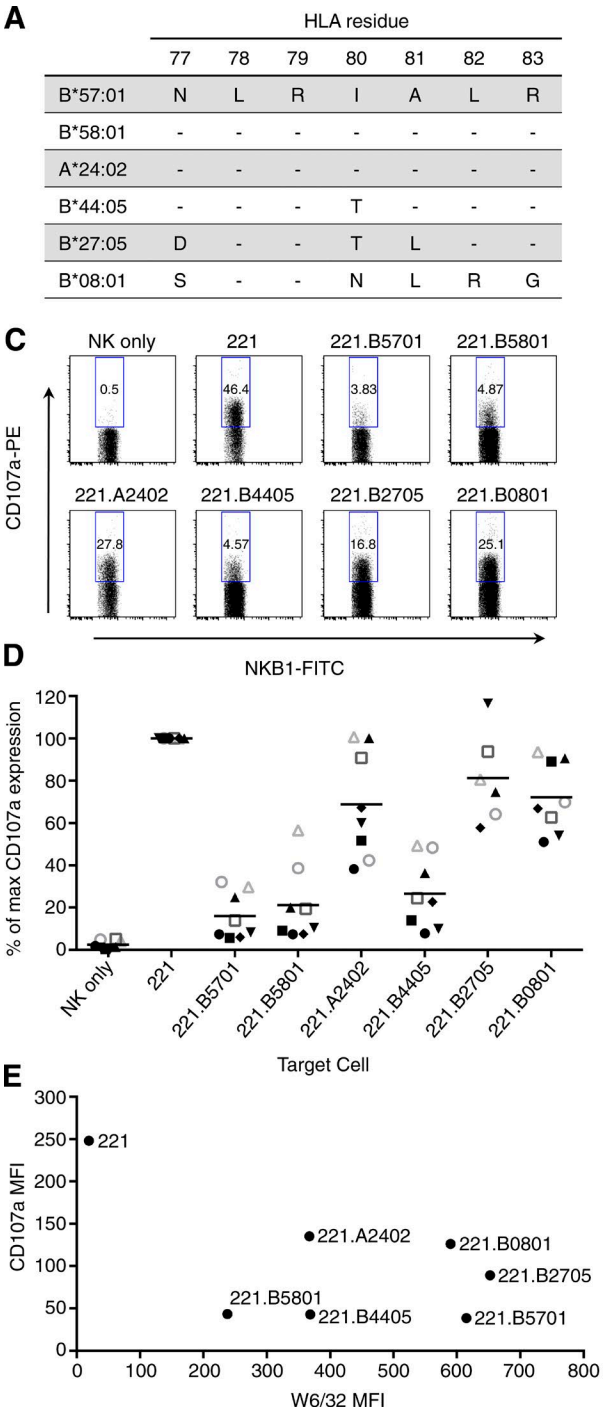

Figure 1. **Inhibition of KIR3DL1$^+$ NK cells varies with HLA-Bw4 expressing targets.** (A) Amino acid sequences across residues 77–83 of transfected HLA-I molecules. (B) The surface expression of transfected HLA-I molecules was confirmed by staining with W6/32 (gray histograms) or anti-Bw4 (black histograms) mAbs followed by anti–mouse IgG-FITC. Filled gray histograms represent background staining with secondary antibody alone. (C and D) KIR3DL1$^+$ NK cells were sorted from eight donors and expanded with IL-2. Equal numbers of KIR3DL1$^+$ NK cells and 221 transfected target cells were cultured with the addition of anti-CD107a for 4 h in the presence of monensin. CD107a expression was then examined by flow cytometry, gating on CD56$^+$/NKB1$^+$ cells. (C) Representative flow cytometric plots showing CD107a expression. Values indicate the percentage of cells expressing CD107a. (D) Normalized CD107a expression after co-culture of KIR3DL1$^+$ NK cells with transfected or parental 221 cells where the response to untransfected 221 cells was adjusted to 100%. Horizontal lines indicate mean. Data are pooled from six independent experiments. (E) The MFI of W6/32 versus the MFI of subsequent CD107a expression is plotted for each 221 transfectant for a representative donor.

(Borrego et al., 1998; Brooks et al., 1999; Petrie et al., 2008). Moreover, variation in the capacity of different HLA-I allotypes to inhibit CD107a expression did not correlate with the level of expression of the transfected HLA-I molecules (Fig. 1 E). Notably, of the cells expressing HLA-Bw4 allotypes, the 221.B5801 transfectants displayed the lowest cell surface expression levels yet had among the most potent inhibitory capacity (Fig. 1, D and E). Similarly, although the expression of HLA-B*27:05 was higher than any other allotype, there was little evidence of Bw4-dependent inhibition of KIR3DL1$^+$ NK cell activation (Fig. 1 D). Possession of Thr80 did not correlate with poor inhibition, as HLA-B*44:05 (Thr80) efficiently inhibited KIR3DL1$^+$ NK cells. Similarly, the presence of Ile80 did not strictly correlate with potent inhibition as although HLA-B*57:01 and -B*58:01 conferred robust inhibition, HLA-A*24:02 was a poor inhib-

itory ligand (Fig. 1 D). Additionally, analyses of the capacity of KIR3DL1$^+$ NK cells to degranulate directly ex vivo revealed a similar pattern of reactivity. Specifically, HLA-B*57:01 was markedly more inhibitory than allotypes such as HLA-A*24:02, indicating that the variation in inhibitory capacity of different HLA-I allotypes was not simply attributable to the use of in vitro–activated NK cells (not depicted). Thus, different HLA-Bw4 molecules displayed variable inhibitory capacities between KIR3DL1$^+$ donors that were not closely correlated with the Ile/Thr dimorphism at position 80. Furthermore, the extent to which distinct HLA-I allotypes, in particular HLA-A*24:02 and HLA-B*27:05, inhibited degranulation of KIR3DL1$^+$ NK cells varied markedly between donors and suggested that allotypic differences in KIR3DL1 also influenced ligand recognition.

KIR3DL1 allotypes demonstrate distinct hierarchies of HLA-Bw4 interaction

To account for the impact of KIR3DL1 polymorphism on HLA-Bw4 recognition and to generate a broader perspective on KIR3DL1–HLA-I binding combinations, soluble KIR3DL1*005, *015, and *001 proteins were produced and used to create fluorescently labeled KIR3DL1 tetramers. These KIR3DL1 tetramers were then assessed for their ability to bind an extensive panel of bead-bound HLA-I molecules comprising 100 distinct allotypes. The 25 HLA-I molecules recognized most strongly by KIR3DL1*015 were then ranked and compared against KIR3DL1*001 and KIR3DL1*005. All three KIR3DL1 tetramers displayed a strong preference for HLA-Bw4 molecules (Fig. 2 A). For example, 19 of the top 25 HLA-I allotypes bound by KIR3DL1*015 were HLA-Bw4 molecules (Fig. 2, B and C). Weak binding was observed to the HLA-C molecules HLA-C*07:02, -C*04:01, -C*01:02, and -C*16:01 (up to 12.7% of the maximum signal for KIR3DL1*015 binding to HLA-C*04:01; Fig. 2, B and C). In contrast, there was negligible binding to HLA-A allotypes, such as HLA-A*02:01, which lacked the Bw4 motif (not depicted). Importantly, the recognition patterns seen in this assay matched well with the data from our degranulation assays where strong recognition of HLA-B*57:01 and B*58:01 allomorphs and weaker recognition of HLA-B*27:05 was observed for all three KIR3DL1 allotypes tested (Fig. 2, A and C).

Each of the KIR3DL1 proteins displayed distinct hierarchical preferences for HLA-Bw4 allomorphs, with KIR3DL1*005 being the most divergent. Although KIR3DL1*001 and *015 exhibited a broadly similar preference for HLA-Bw4 allomorphs, differences were apparent (Fig. 2, A–C). For example, KIR3DL1*001 bound more strongly than KIR3DL1*015 to several HLA-Bw4 allomorphs, including HLA-B*44:03 and HLA-B*57:03. Moreover, KIR3DL1*001 bound HLA-B*57:01 and HLA-B*57:03 with similar intensity, whereas KIR3DL1*015 preferentially bound HLA-B*57:01 in comparison with HLA-B*57:03. Thus, there were clear differences between KIR3DL1*001 and *015 in terms of relative binding strength across different HLA-Bw4 allomorphs and ultimately in the rank order of binding.

Although KIR3DL1*005 bound HLA-I allotypes such as HLA-B*57:01 and HLA-B*58:01 with high avidity, there were several significant changes in both the rank order of binding and ligand specificity in comparison with both KIR3DL1*001 and KIR3DL1*015 (Fig. 2, B and C). For example, KIR3DL1*001 and *015 bound HLA-A*32:01 very strongly, yet there was only a weak interaction with HLA-A*24:02. In contrast, the binding of KIR3DL1*005 to HLA-A*24:02 and HLA-A*32:01 was equivalent, indicating broader recognition of HLA-A allomorphs possessing the Bw4 motif (Fig. 2 C). Additionally, there was substantial variation in KIR3DL1 binding to certain HLA-B allotypes, most notably HLA-B*44:02 and -B*44:03, the former of which was ranked second for KIR3DL1*005 binding, yet interacted relatively poorly with *001 and *015. This overall comparison against KIR3DL1*001 and *015 shows that *005 has both broader and distinct preference for HLA-Bw4 ligands.

This broad screening approach allowed the impact of the Ile/Thr dimorphism at position 80 of HLA-Bw4 allotypes on KIR3DL1 binding to be reexamined (Fig. 2, B and C). When viewed as a group, Ile80$^+$ allotypes preferentially interacted with both KIR3DL1*001 and *015 relative to the Thr80$^+$ allotypes (Fig. 2, A and B). Nevertheless, the presence of Ile80 did not strictly correlate with strong binding to either KIR3DL1*001 or *015 because HLA-A*24:03 and -B*52:01 (Ile80) interacted more weakly than HLA-B*44:03 and HLA-B*47:01 (Thr80; Fig. 2, A and C). In contrast, there were no significant differences in the ability of KIR3DL1*005 to discriminate between allotypes that contain Ile80 and Thr80 (Fig. 2 B). These data reveal substantial variation in the specificity between KIR3DL1 allotypes, with KIR3DL1*005 being the most permissive allotype across the range of HLA-Bw4 molecules. Moreover, the Ile80/Thr80 dimorphism of HLA-Bw4 allotypes is not predictive of the strength of ligand recognition by KIR3DL1.

Differences in HLA-Bw4–mediated inhibition between KIR3DL1$^+$ NK cell clones

Although the interaction of KIR3DL1 tetramers to beads coated with individual HLA-I allotypes generated binding hierarchies for KIR3DL1*005, *015, and *001, it was unclear whether these reflected functional differences. Consequently, a panel of NK clones from donors of known KIR3DL1 allotype, LM (*KIR3DL1*001*), RM (*KIR3DL1*002* and **00501*), and BC (*KIR3DL1*00501*), were generated, with the KIR3DL1*002 and *005 populations of donor RM isolated by sorting DX9^{hi} and DX9^{lo} NK cells, respectively (not depicted). KIR3DL1*002 belongs to the **015* lineage, differing from KIR3DL1*015 only at position 238 within the D2 domain (Fig. 3 A). These clones were then assessed for their capacity to lyse either 221 cells or 221 cells transfected with different HLA-I allotypes. Consistent with both their

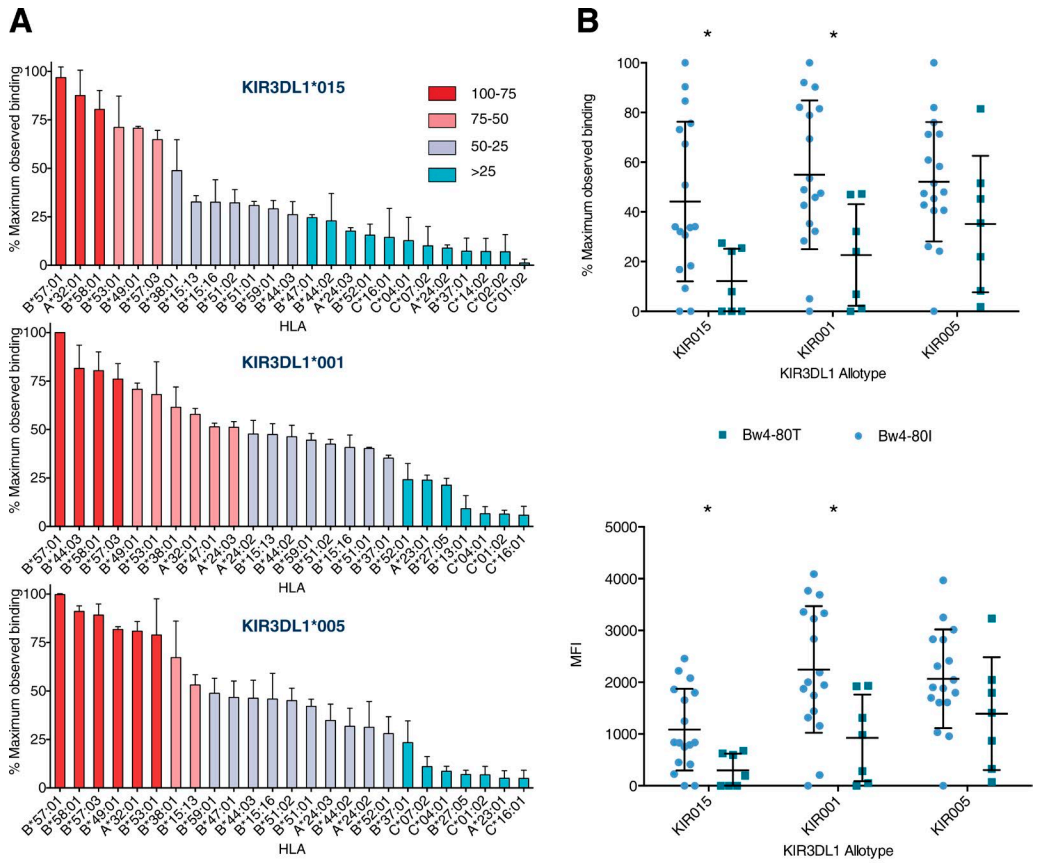

C

HLA	Bw Subtype	KIR015	KIR001	KIR005
B*57:01	Bw4 80I	96.8	99.7	100
A*32:01	Bw4 80I	87.6	80.9	57.9
B*58:01	Bw4 80I	80.4	91.1	80.4
B*53:01	Bw4 80I	71.2	78.9	68.1
B*49:01	Bw4 80I	70.7	81.8	70.8
B*57:03	Bw4 80I	64.8	89.1	76.0
B*38:01	Bw4 80I	48.8	67.3	61.5
B*15:13	Bw4 80I	32.6	53.1	47.4
B*15:16	Bw4 80I	32.5	45.9	40.7
B*51:02	Bw4 80I	32.2	45.0	42.4
B*51:01	Bw4 80I	30.8	42.1	40.2
B*59:01	Bw4 80I	29.1	48.9	44.5
B*44:03	Bw4 80T	26.1	46.3	81.5
B*47:01	Bw4 80T	24.5	46.6	51.4
B*44:02	Bw4 80T	22.9	31.8	46.2
A*24:03	Bw4 80I	17.6	34.8	51.2
B*52:01	Bw4 80I	15.5	28.0	24.1
C*16:01	C1 N	14.4	4.87	5.84
C*04:01	C2 K	12.7	8.55	6.59
C*07:02	C1 N	10.0	11.0	5.62
A*24:02	Bw4 80I	8.91	31.2	47.7
B*37:01	Bw4 80T	7.24	23.4	35.2
C*14:02	C1 N	7.06	4.42	5.45
C*02:02	C2 K	6.90	4.13	4.17
C*01:02	C1 N	1.14	6.72	6.43
A*23:01	Bw4 80I	0.00	4.95	23.9
B*27:05	Bw4 80T	0.00	6.92	21.3
B*13:01	Bw4 80T	0.00	0.00	9.12

HLA	Bw Subtype	KIR015	KIR001	KIR005
B*57:01	Bw4 80I	1	1	1
A*32:01	Bw4 80I	2	5	8
B*58:01	Bw4 80I	3	2	3
B*53:01	Bw4 80I	4	6	6
B*49:01	Bw4 80I	5	4	5
B*57:03	Bw4 80I	6	3	4
B*38:01	Bw4 80I	7	7	7
B*15:13	Bw4 80I	8	8	12
B*15:16	Bw4 80I	9	12	16
B*51:02	Bw4 80I	10	13	15
B*51:01	Bw4 80I	11	14	17
B*59:01	Bw4 80I	12	9	14
B*44:03	Bw4 80T	13	11	2
B*47:01	Bw4 80T	14	10	9
B*44:02	Bw4 80T	15	16	13
A*24:03	Bw4 80I	16	15	10
B*52:01	Bw4 80I	17	18	19
C*16:01	C1 N	18	25	25
C*04:01	C2 K	19	21	23
C*07:02	C1 N	20	20	26
A*24:02	Bw4 80I	21	17	11
B*37:01	Bw4 80T	22	19	18
C*14:02	C1 N	23	26	27
C*02:02	C2 K	24	27	28
C*01:02	C1 N	25	23	24
A*23:01	Bw4 80I	N/A	24	20
B*27:05	Bw4 80T	N/A	22	21
B*13:01	Bw4 80T	N/A	N/A	22

Figure 2. **Tetramers of each KIR3DL1 allomorph display distinct binding preferences to HLA-I–coated beads.** (A) The fluorescent values for the top 25 HLA alleles binding to each KIR3DL1 allotype in the HLA-I bead assay are shown as normalized values for KIR3DL1*015, KIR3DL1*001, and KIR3DL1*005. HLAs are categorized by percentage maximum binding with 100–75% maximum binding (red), 75–50% maximum binding (pink), 50–25% maximum binding (gray), and 25–0% binding (teal). (B) KIR3DL1 allotype recognition for all HLA-Bw4–containing allomorphs present on the bead assay is plotted

superior capacity to bind KIR3DL1 tetramers (Fig. 2 C) and to inhibit the activation of polyclonal NK cells (Fig. 1 D), the expression of HLA-B*57:01 and HLA-B*58:01 conferred protection from all KIR3DL1$^+$ NK cell clones assessed, regardless of KIR3DL1 allotype (Fig. 3 B). This protection was mediated in part through KIR3DL1, as indicated by the increased lysis after addition of the KIR3DL1/S1-specific antibody, Z27. Similarly, the expression of HLA-B*44:05 also conferred substantial target cell protection irrespective of KIR allotype, again reflecting our observations in assays of bulk NK cell cultures (Figs. 1 D and 3 B).

In contrast, NK cell clones expressing either KIR3DL1*001 or KIR3DL1*002 readily lysed 221 cells expressing HLA-A*24:02, whereas the same HLA-I allotype conferred protection from clones expressing KIR3DL1*005 (Fig. 3 B). The extent of this inhibition varied between KIR3DL1*005$^+$ donors, with donor BC exhibiting ∼40% maximum lysis compared with donor RM at 18%. The pattern of reactivity of NK cell clones toward target cells expressing HLA-B*27:05 was similar to those that expressed HLA-A*24:02, in that although HLA-B*27:05 did not confer significant protection from clones expressing KIR3DL1*002, it nevertheless conferred significant protection from lysis by clones from donor RM that expressed the *005 allotype. This broadly reflected what was observed in the KIR3DL1 tetramer binding assay because KIR3DL1*005 bound to both HLA-A*24:02– and HLA-B*27:05–coated beads more strongly than the other KIR3DL1 allotypes, albeit with weaker avidity than was observed for HLA-B*57:01, -B*58:01, and -B*44:02. Nevertheless, the binding of KIR3DL1*005 to HLA-B*27:05 was still stronger than that to any non-Bw4 allotype. Collectively, the functional and bead binding data suggest that although HLA-B*27:05 may interact with KIR3DL1*005 with low avidity, it is still able to function as a ligand. In contrast, KIR3DL1*001 and **015*-lineage molecules appear to have a higher binding threshold for functional ligand recognition.

To confirm and extend these analyses, an additional panel of clones was established from another four donors. The KIR3DL1 allele expressed in each clone was determined by sequencing KIR3DL1 cDNAs amplified from RNA, identifying clones expressing KIR3DL1*005 and *015, as well as KIR3DL1*002 and *009. Uniquely, KIR3DL1*009 possesses the D0 domain of KIR3DS1 coupled with the *001 D1–D2 domains (Fig. 3 A) and has been suggested to display weaker binding to HLA-Bw4 than KIR3DL1*001 or *005 (Mulrooney et al., 2015). These NK cell clones were then cocultured with either parental or HLA-I–transfected 221 cells, and the expression of CD107a was assessed by flow cytometry. The expression of CD107a by KIR3DL1*001$^+$, *002$^+$, and *005$^+$ NK clones was consistent with the data obtained from the cytotoxicity assays (Fig. 3 C). Namely, HLA-B*57:01, HLA-B*58:01, and HLA-B*44:05 effectively inhibited degranulation by all KIR3DL1 allotypes tested, whereas HLA-A*24:02 only inhibited activation of the KIR3DL1*005$^+$ clone. Both KIR3DL1*015 and *009 resembled KIR3DL1*001 in their recognition of HLA-B*57:01, HLA-B*58:01, and HLA-B*44:05, where all three HLA-I allotypes inhibited CD107a expression. In contrast, the expression of HLA-A*24:02 had only a modest inhibitory impact on degranulation of NK cell clones expressing KIR3DL1*001, *002, *015, and *009. Collectively, the data derived from the analyses of 35 NK clones derived from seven donors expressing a range of KIR3DL1 allotypes have identified clear specificity differences between KIR3DL1*005, and several KIR3DL1 allotypes that share common polymorphisms across the D1 and D2 domains, notably residues 182 and 283. The data highlight that the Bw4 recognition preferences of KIR3DL1 do not simply segregate with the presence of an Ile or Thr at position 80. Moreover, the data suggest that KIR3DL1*005 has an expanded ligand range relative to allotypes of the KIR3DL1*015 lineage or the recombinant allotypes KIR3DL1*001 and *009. Accordingly, there is a functional hierarchy of HLA-Bw4 recognition that is dependent on KIR3DL1 polymorphism.

Molecular basis of KIR3DL1 polymorphism on HLA-I recognition

To provide molecular insights into the altered patterns of ligand recognition by KIR3DL1*001, *005, and *015, the structures of KIR3DL1*005 and *015 in complex with HLA-B*57:01 were determined to 2.3 and 2.5 Å, respectively (Table 1). The KIR3DL1 complexes were crystallized in the same conditions and in the same space group (Table 1). The high quality of the resultant structures allowed for direct comparison with the previously determined KIR3DL1*001–peptide–HLA-B*57:01 complex (Vivian et al., 2011). The overall binding mode of these three KIR3DL1–peptide–HLA-I ternary complexes was similar. Specifically, the D0 domain clamped around the side of HLA-B*57:01, abutting β2-microglobulin, whereas the D1 and D2 domains were positioned above the C-terminal end of the peptide-binding cleft, with the D1 domain interacting with the Bw4 motif (Fig. 4, A and B). The

and separated by dimorphism at position 80 (80I and 80T). Binding values are given as normalized binding (top) and MFIs (bottom). Significant differences between Bw4 80I and Bw4 80T subtype recognition as measured by independent multiple Student's *t* tests are shown with an asterisk. The p-value for KIR3DL1*001 is 0.016 and that for KIR3DL1*015 is 0.019, whereas the nonsignificant value for KIR3DL1*005 is 0.143. (C) HLA-I alleles on the bead assay are ranked by recognition of KIR3DL1*015, and the top 28 alleles are depicted with comparison of rank and binding values for these alleles with those for the KIR3DL1*001 and *005 allotypes. HLAs are shown by rank (left) and percentage (right) of highest binding allele. All data represent mean values from three independent experiments. Error bars depict one standard deviation from the mean value. Shading is a three-color conditional formatting scale. A percentage of maximum binding value of 0 is assigned blue and that of 100 is assigned red, and the 50th percentile is colored light pink.

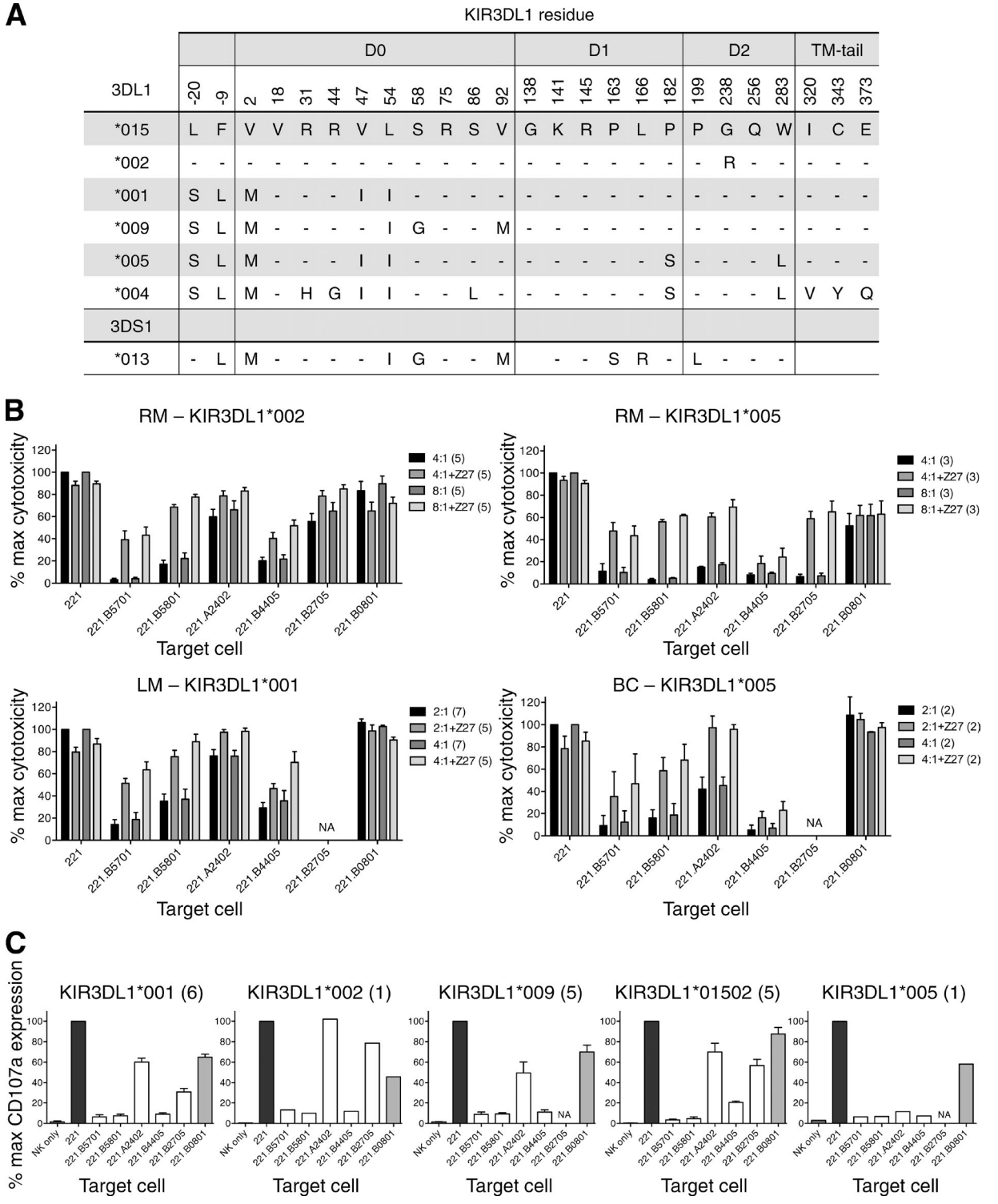

Figure 3. **KIR3DL1 molecules of different lineages functionally discriminate between HLA-Bw4 ligands.** (A) The polymorphic residues found in KIR3DL1*015, *002, *001, *009, *005, and *004 (and the KIR3DS1 lineage) are shown, with additional residues of variance also noted (list is not exhaustive). (B) KIR3DL1^{+} NKG2A^{-} cells were sorted and cloned from three healthy volunteers of known KIR3DL1 allotype (LM *001; RM *002/*00501; BC *00501). Cloned NK cells were then incubated with ^{51}Cr-labeled 221 transfectants at the indicated E:T ratios in the presence or absence of anti-KIR3DL1/S1 mAb (Z27). Data shown are mean cytotoxicity ± SEM, where the response to untransfected 221 cells was adjusted to 100%, based on the maximal cytotoxicity observed in the presence of parental 221 targets and in the absence of Z27. The number of clones individually assessed at the given ratios is noted in parentheses.

KIR3DL1*005 and *015 complexes maintained key contacts with HLA-B*57:01 that were identified from structural and mutagenesis studies of KIR3DL1*001 recognition (Vivian et al., 2011). In particular, the interactions between positions Phe9 on the D0 domain and residues 17–19 on HLA-B*57:01 and the interactions between Tyr200, Phe276, and Glu282 on the D2 domain and residue Lys146 on the α2 helix of HLA-B*57:01 were conserved (Fig. 4 B). Similarly, the contacts between the KIR3DL1 residue Leu166 and Ile80 in the Bw4 motif and Ser8 in the bound peptide were preserved across all KIR3DL1 ternary complexes (Fig. 4 B). The total buried surface area at the complex interfaces was also comparable, (KIR3DL1*001 = 1,790 Å^2, *005 = 1,870 Å^2, and *015 = 2,060 Å^2). Accordingly, the three KIR3DL1 allomorphs use a similar inventory of principal residues to recognize HLA-B*57:01 complexed with the LSSPVTKSF (LF9) peptide.

Despite this consensus docking mode, differences were observed between the three ternary complexes attributable to polymorphic residues that distinguish KIR3DL1*001, *005, and *015. KIR3DL1*005 and *015 differ at seven amino acids, five in the signal sequence–D0 domain and two in the D1–D2 domains. Across the extracellular regions examined, KIR3DL1*015 differs from *005 at positions Val47Ile, Leu54Ile, Pro182Ser, and Trp283Leu. As KIR3DL1*001 is a recombinant of the D0 from *005 and the D1–D2 from *015, it thus differs from *015 at positions 47 and 54 and from *005 at positions 182 and 283 (Fig. 4 A).

The docking of the D0 and D1 domains to HLA-B*57:01-LF9 was distinct between the complexes, despite a common 80° hinge angle about the D0–D1 domains (Fig. 4, C and D). Notably, the KIR3DL1*005 D0–D1 domain arrangement was identical to that observed in *015, both of which were distinct from that of *001. More specifically, compared with the KIR3DL1*001 complex, the *005 and *015 complexes displayed a 3° difference in the crossing angle of the D1 domain and a 1-Å translational shift of the D0 domain. These two D0–D1 profiles were coincident with two distinct conformations of the C–C′ loop (Fig. 5 A). Such conformations were also observed in complexes of KIR3DL1*001 with HLA-B*57:01 bound to different peptides (unpublished data). Thus, the C–C′ loop conformation varies as a function of both the bound peptide and the KIR3DL1 allotype.

The hinge angle between the D1 and D2 domains clearly distinguished the KIR3DL1*001 and *015 complexes from that of *005. This angle in KIR3DL1*001 and *015 was more acute (76°) than that observed in *005 (80°; Fig. 4, C and D). Centrally placed to influence the interdomain hinge angle was the dimorphic residue 283, residing on the F′ strand of the D2 domain, interconnecting the D1 and D2 domains. Trp283 in KIR3DL1*001 and *015 and Leu283 in *005 were positioned in a hydrophobic pocket and made similar contacts to neighboring residues, including contacts to Leu112 and Val195 on the D1 domain and His233, Phe273, and Ser275 on the D2 domain (Fig. 5, B and D). Unique to Trp283 was an H-bond from the indole nitrogen to Pro280 that aided the alignment of Trp283. These contacts were of importance to the hinge angle, with Trp283 oriented parallel to the axis of the D1–D2 hinge. Trp283 therefore had a narrower profile than Leu283, allowing for a tighter hinge angle (Fig. 4 C and Fig. 5, B and D).

The differences in the relative angles of the KIR3DL1 domains had a modest impact on contacts with HLA-B*57:01–LF9. Indeed, all contacts were preserved to residues known to be critical for the interaction with KIR3DL1*001 (Vivian et al., 2011). However, differences were observed at the short helix between the E–F strands, as Met165 on KIR3DL1*005/*015 formed an additional peptide contact to Thr6. Furthermore, the 8° difference in the crossing-angle of the D2 domain (Fig. 4, C and D) enabled additional contacts between the F-strand residue His278 on KIR3DL1*001/*015 and Ile142 and Tyr84 of the HLA molecule (Fig. 5 C). Combined with the wider hinge angle for the D1–D2 domains of KIR3DL1*005, this translates to a different docking mode for the *005 allotype, which further associates with an impact on HLA-Bw4 recognition.

Increased mobility of ligand-binding loops within KIR3DL1*005

We hypothesized that the wider D1–D2 angle in KIR3DL1*005 relative to either *001 or *015 would confer a greater degree of flexibility around the peptide–HLA-I binding site, thereby allowing KIR3DL1*005 to tolerate a broader range of ligands. To test this hypothesis, solution phase deuterium exchange experiments were performed on KIR3DL1*001, *015, and *005. In these experiments, increased levels of hydrogen exchange with deuterium were associated with a greater degree of mobility. Strikingly, mass spectrometric analysis showed that the greatest difference in the extent of deuterium exchange was located within ligand-binding loops of KIR3DL1 (Fig. 6, A–C). These loops were the D1 C–C′ loop (residues 133–145; Fig. 6 A), the D1 E–F loop (residues 160–173; Fig. 6 B), and the D1–D2 hinge loop (residues 194–205; Fig. 6 C). Moreover, in each case, there was significantly more deuterium exchange in

Data shown are pooled from six independent experiments. (C) PBMCs were isolated from unknown donors, KIR3DL1$^+$ cells were sorted and cloned, and the KIR3DL1 alleles were sequenced. Expanded NK clones were incubated with 221 transfectants at a 1:1 ratio with the addition of a CD94-specific blocking mAb Y9, along with anti-CD107a, followed by monensin. After 4-h incubation, cells were stained for CD56 and KIR3DL1, and CD107a expression was assessed by flow cytometry. Experiments were performed once for each clone with the CD107a expression normalized to the maximal CD107a expression observed after co-culture in the presence of untransfected 221 cells. Plot shows mean CD107a expression ± SEM with the number of clones assessed noted in parentheses. Data were pooled from five independent experiments.

Table 1. **Refinement statistics for KIR3DL1*005 and KIR3DL1*015**

Statistics	KIR3DL1*005–HLA-B*57:01–LF9	KIR3DL1*015–HLA-B*57:01–LF9
Data collection statistics		
Temperature (K)	100	100
X-ray source	MX2 Australian synchrotron	MX2 Australian synchrotron
Space group	*P*1	*P*1
Cell dimensions	*a* = 51.6, *b* = 61.3, *c* = 66.4 α = 95.2, β = 100.2, γ = 108.2	*a* = 51.6, *b* = 61.1, *c* = 65.1, α = 95.6, β = 98.5 γ = 108.6
Resolution (Å)	50–2.30 (2.42–2.30)	50–2.5 (2.64–2.50)
Total no. observations	139,081 (20,784)	99,352 (14,846)
No. unique observations	30,955 (4,571)	23,125 (3,419)
Multiplicity	4.5 (4.5)	4.3 (4.3)
Data completeness (%)	92.9 (95.0)	90.7 (91.5)
$1/\sigma_I$	6.9 (3.6)	7.3 (3.7)
R_{merge}[a]	0.144 (0.421)	0.188 (0.897)
Refinement statistics		
Nonhydrogen atoms		
Protein	5,260	5,294
Water	230	148
R_{factor}[b]	0.20	0.18
R_{free}[b]	0.25	0.23
rmsd from ideality		
Bond lengths (Å)	0.003	0.005
Bond angles (°)	0.702	0.874
Ramachandran plot		
Favored regions (%)	95.0	95.4
Allowed regions (%)	5.0	4.6
B-factors		
Mean main chain (Å2)	34	32
Mean side chain (Å2)	38	37
Mean water (Å2)	38	36

[a] $R_{merge} = \sum_{hkl} \sum_i |I_{hkl,i} - \langle I_{hkl} \rangle| / \sum_{hkl} \sum_i I_{hkl,i}$.
[b] $R_{factor} = \sum_{hkl} ||F_o| - |F_c|| / \sum_{hkl} |F_o|$ for all data excluding the 5% that comprised the R_{free} used for cross-validation.

KIR3DL1*005 relative to *001 or *015 (Fig. 6, A–C). The extent of exchange in the latter two allotypes was similar. Deuterium exchange data were also collected on peptide fragments from the D2 C–C′–D strands and the D–E loop (residues 233–253; Fig. 6 D), the D2 E–F loop and F-strand (residues 260–274; Fig. 6 E), and the D2 F–F′ and F′–G loops (residues 275–292; Fig. 6 F). For each of these D2 peptide fragments, there was no difference in the extent of deuterium exchange. Collectively, these data show that the ligand-binding loops of the D1 and the D1–D2 hinge loop of KIR3DL1*005 are more dynamic than either *001 or *015, suggesting that the wider hinge angle ultimately allows the *005 allotype to adopt conformations that can accommodate microvariation in ligand structure resulting from both HLA-I polymorphism and variability in the associated peptide repertoire.

DISCUSSION

High-avidity interactions between inhibitory KIRs and their HLA-I ligands are thought to result in well-educated NK cells with potent effector functions that are highly responsive to cells with reduced surface expression of HLA-I. Such interactions have been proposed to be associated with poor outcomes in malignancies such as AML, where there is little evidence of HLA-I down-regulation, and with improved viral control in HIV-infected individuals (Cooley et al., 2014; Marra et al., 2015). However, the molecular signatures that define "high-affinity" interactions are themselves poorly defined. Specifically with respect to KIR3DL1, the presence of an Ile80 within the Bw4 motif has been thought to act as a signature for potent ligands, particularly for KIR3DL1 allotypes with high levels of cell surface expression, which ultimately translated into clinical associations with disease progression in the setting of HIV (Cella et al., 2000; Yawata et al., 2006; Martin et al., 2007). Several studies following a similar approach have found associations between the presence of KIR3DL1 and $Bw4^{80I}$ allotypes with the probability of relapse in patients receiving hematopoietic stem cell transplantation for AML or simply with the presence of $Bw4^{80I}$ in diseases such as Behçet's disease and hepatitis B–associated hepatocellular carcinoma, often in association with *KIR3DS1* (Pan et al., 2011; Kuranov et al., 2014; Marra et al., 2015). Although residue 80 clearly plays a central role in KIR3DL1 recognition, the functional and binding data presented here demonstrate that the presence of Ile80 alone is insufficient for strong engagement of KIR3DL1. Notably, there were marked differences between different $Ile80^+$ Bw4 allotypes in terms of their capacity to inhibit target cell lysis by clonal or polyclonal $KIR3DL1^+$ NK cells. For example, although HLA-B*57:01 and HLA-B*58:01 readily conferred protection from lysis by $KIR3DL1^+$ NK cells, HLA-A*24:02 exhibited considerably

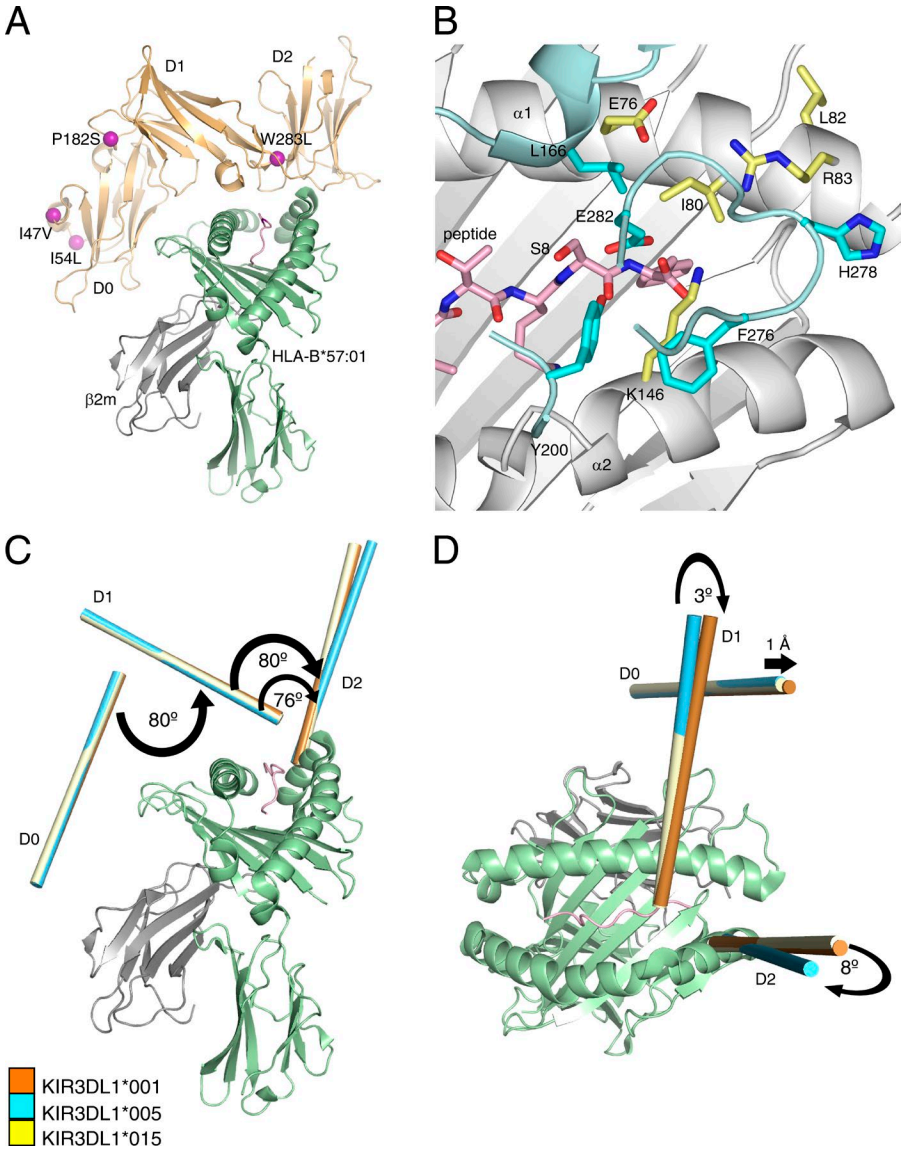

Figure 4. **Structural comparison of KIR3DL1 allomorphs in complex with HLA-B*57:01.** (A) The location of the polymorphic differences between KIR3DL1*001, *005, and *015 mapped onto the structure of KIR3DL1*005 in complex with HLA-B*57:01. (B) The primary contacts between the KIR3DL1 (cyan) and HLA-B*57:01. The Bw4 motif on the α1 helix and Lys146 on the α2 helix are shown as yellow sticks. The peptide is shown as pink sticks. (C and D) Docking of KIR3DL1 allotypes onto HLA-B*57:01–LF9. The axes of inertia of each of the KIR3DL1 domains are shown as rods. KIR3DL1*001 is colored orange, *005 is colored cyan, and *015 is colored yellow. The hinge angles between the domains are shown in C and the crossing angles of the domains in D.

weaker effects, despite the fact that all three HLA-I allotypes shared an identical sequence spanning the Bw4 motif. Extending these functional observations, our broad screening of HLA-I binding preferences using KIR3DL1 tetramers showed that although Bw4 molecules possessing Ile80 were among the best ligands regardless of KIR3DL1 allotype, several Ile80^{+} allotypes such as HLA-A*23:01, HLA-A*24:02, and HLA-B*52:01 were poorly recognized. Indeed, these allotypes were weaker ligands than HLA-B*44:02, HLA-B*44:03, and HLA-B*47:01, all of which encode Thr80. Thus, although many potent ligands possess Ile80, the Ile/Thr dimorphism at residue 80 cannot strictly be used as a marker of KIR3DL1 ligand affinity. This has important implications for disease association studies based around the presence or absence of Bw4 allotypes that have Ile80. The majority of Bw4^{80I} alleles that act as high-avidity ligands for KIR3DL1 are themselves relatively common, at least in certain ethnicities. For example, the overall frequency of HLA-B*57:01 is typically reported to vary between 1 and 3% in most studies but may be significantly higher in those of Indian decent, whereas the overall frequency of HLA-B*58:01 is ∼3% and can be very common in African populations (Cao et al., 2001; Solberg et al., 2008). However, we have shown that other Bw4^{80I} alleles such as HLA-A*24:02 and -B*52:01, both of which can be very common (>5%) in certain Asian populations, can be relatively poor ligands, at least for certain KIR3DL1 allotypes (Cao et al., 2001; Solberg et al., 2008). The inclusion of the latter alleles into groups of alleles that are considered to be high avidity/function may mean the strength of the associations reported with diseases in HIV and AML are underestimated. Similarly, the exclusion of common Bw4^{80T} allotypes such as HLA-B*44:03 that interact robustly with KIR3DL1*015, *001, and *005 may also serve to diminish the statistical strength of these disease associations. As

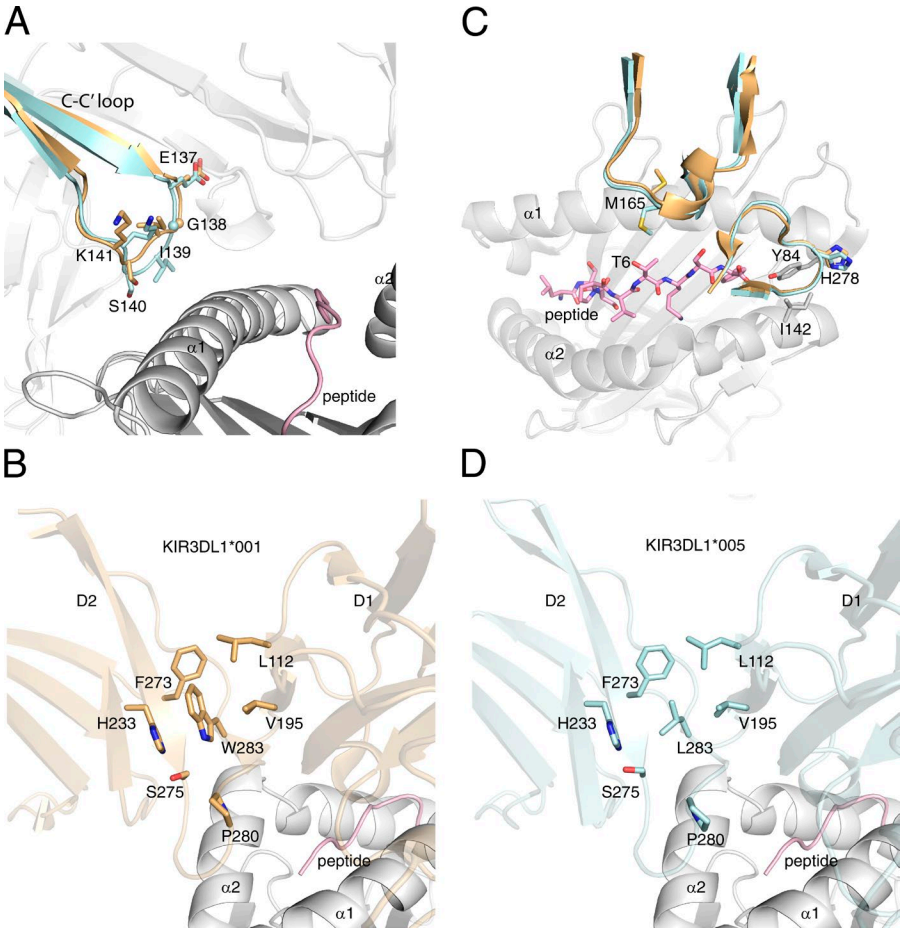

Figure 5. **Structural details underpinning the differences between KIR3DL1 allomorphs in complex with HLA-B*57:01.** (A) Two conformations of the C–C′ loop of KIR3DL1 are present in complex with HLA-B*57:01. The loop as observed in the KIR3DL1*001 complex is colored orange, and the conformation as observed in *005/*015 is colored blue. (B and D) The structural consequences surrounding the site of the KIR3DL1 W283L dimorphism at the D1–D2 interface. The conformation as observed in KIR3DL1*001/*015 is shown in B. The conformation as observed in KIR3DL1*005 is shown in D. (C) Subtle differences at positions Met165 and His278 differentiate the binding of KIR3DL1*001 and *005. The conformation as observed in KIR3DL1*001/*015 is colored orange, whereas the conformation as observed in *005 is colored cyan.

such, the data here provide an empirical rationale for the re-evaluation of disease association studies that are genuinely based on the avidity of the KIR3DL1/ligand.

Further compounding the difficulty of interpreting associations of KIR3DL1 and Bw4 alleles with clinical outcomes is allelic variation in *KIR3DL1* itself. Our data, based on the binding of KIR3DL1 allotypes representative of the two major inhibitory allelic lineages (*015 and *005) along with an interlineage recombinant (*001), systematically evaluated the extent to which allotypic variation in KIR3DL1 modulates receptor specificity. Notably, KIR3DL1*015 bound to its ligands with lower avidity than either *001 or *005. Moreover, the polymorphic differences between KIR3DL1*001 and *015 did not simply impact the overall level of binding but rather resulted in subtle differences in the specificity between KIR3DL1*015 and *001. More striking still were the differences in binding profile between KIR3DL1*005 and both KIR3DL1*001 and *015. Not only did KIR3DL1*005 bind a greater range of HLA-I allotypes, but there were also marked differences in the hierarchy of HLA-I allotype binding. When assessed in functional assays using NK cell clones, the altered binding hierarchy between different KIR3DL1 allotypes was manifest in an altered specificity. Namely, a larger spectrum of HLA-I allotypes were able to inhibit activation of NK cell clones expressing KIR3DL1*005 compared with other allotypes examined, including KIR3DL1*001, *015, *009, and *002.

Previous findings had suggested that the Trp/Leu dimorphism at residue 283 of KIR3DL1 was critical in defining the *015 and *005 lineages of KIR3DL1 and show that the introduction of Leu283 in KIR3DL1*001, *007, and *015 enhanced binding to Bw4 tetramers possessing Thr80 (Sharma et al., 2009; O'Connor et al., 2014). Here we show that KIR3DL1 allotypes possessing Trp283 had a more restricted range of ligands as assessed by both binding and functional experiments than KIR3DL1*005, which possesses a Leu at this position. The differences between KIR3DL1*015, *001, and *005 center on a limited set of dimorphic residues: residues 2, 47, and 54 on the D0 domain (distal to the HLA binding interface), residue 182 on the D1 domain (at the D0–D1 domain interface), and residue 283 (at the D1–D2 domain interface). Sharma et al. (2009) have shown that KIR3DL1*001 bound more strongly to HLA-A*24:02 tetramers complexed with a nef-encoded peptide than either KIR3DL1*005 or KIR3DL1*015, suggesting some degree of synergy between the D0 and D1–D2 domains in the recombinant allele. However, given that ligand recognition by KIR3DL1 is acutely dependent on the sequence of the

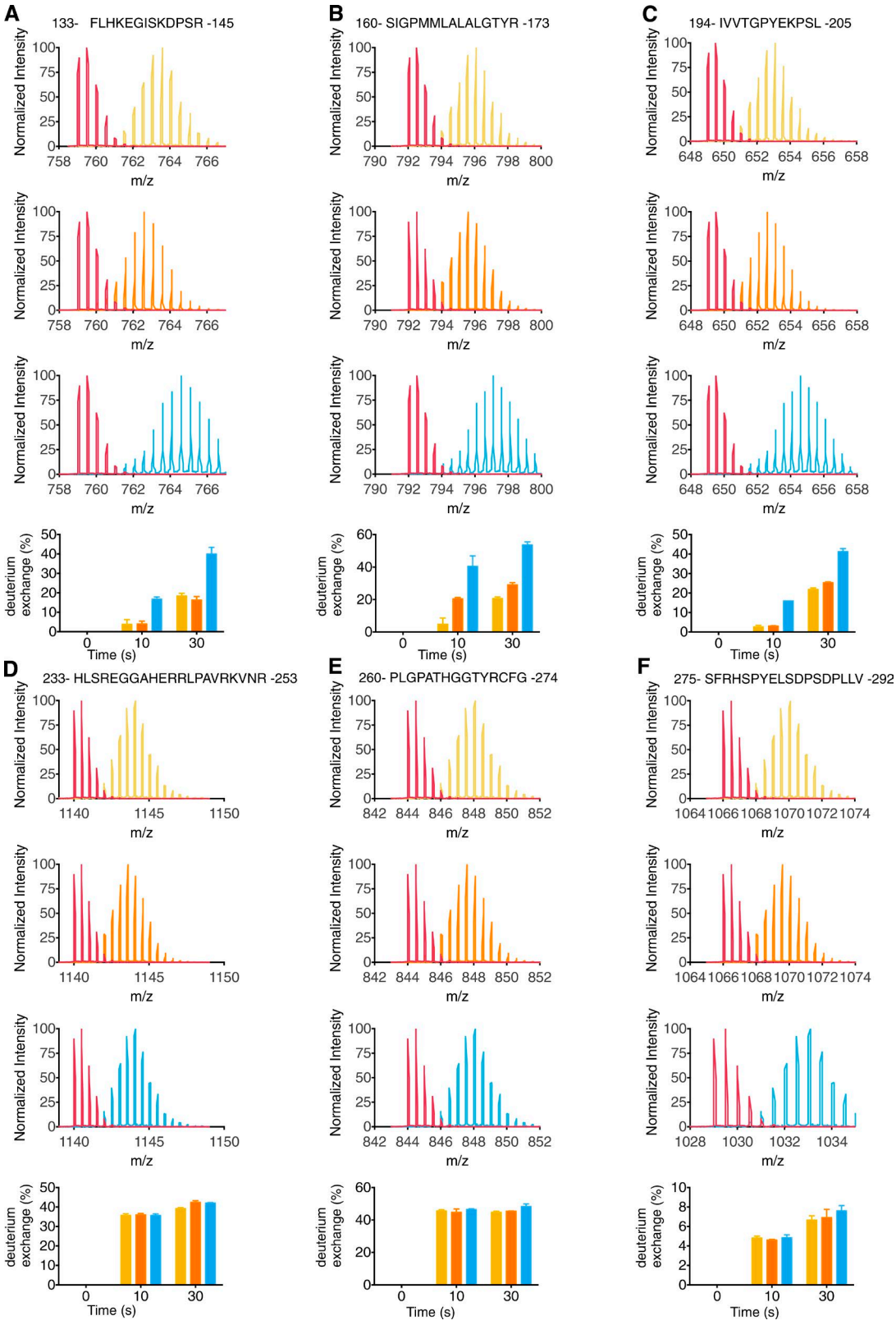

HLA-associated peptide, it is unclear whether this synergism was a general feature of ligand recognition by these allotypes (Malnati et al., 1995; Thananchai et al., 2007). Regardless, that polymorphisms distal to the HLA-binding interface are able to impact ligand binding avidity implies an indirect molecular mechanism. Several studies have noted such effects, particularly from allotypes bearing polymorphisms at residues 58, 92, and 238 (Carr et al., 2005; Thananchai et al., 2007; Mulrooney et al., 2015). Interestingly, our data analyzing the structures of KIR3DL1*001, *005, and *015 identified two conformations of the D0–D1 domains. However, these differing docking conformations were not wholly attributable to KIR3DL1 polymorphisms as different docking angles have been observed between KIR3DL1*001 and HLA-B*57:01 in complex with different peptides (unpublished data). This indicates that there is a degree of flexibility across the three KIR3DL1 domains whose ultimate arrangement, though in part regulated by polymorphic residues that are spatially remote from the ligand-binding site, are also subject to the nature of the HLA allotype and the associated peptide.

The structural data show that the Leu-Trp dimorphism at position 283 is associated with an altered juxtapositioning of the D1 and D2 domains, resulting in a subtle realignment of the residues contacting the HLA-B*57:01–LF9 complex. Moreover, the deuterium exchange data revealed that the larger hinge angle associated with the presence of Leu283 confers a degree of flexibility, particularly over the KIR3DL1 loops, which are intimately involved in recognition of both the peptide and the Bw4 motif. These findings suggest that the increased flexibility of the ligand-binding region allows KIR3DL1*005 to better accommodate variability in the sequence of peptides bound to Bw4 allotypes. Consistent with this notion, the introduction of Leu283 into both KIR3DL1*001 and *015 substantially enhanced binding to HLA-B*57:01 complexed with an escape variant of the HIV-encoded peptide TW10 (O'Connor et al., 2014).

Predicting the functional outcomes that result from KIR3DL1–HLA-I interactions is complex and is likely based on the conjoined effects of avidity and surface expression of both receptor and ligand, as well as cell surface clustering and the signaling potential of the receptor (Pando et al., 2003; Carr et al., 2005; Mulrooney et al., 2015). Although it is clear that several polymorphisms in KIR3DL1 can impact functional responses to cells bearing HLA-Bw4 molecules, our study has elucidated the effect of polymorphisms within the two major KIR3DL1 lineages that combine to influence binding avidity and ultimately specificity. Accordingly, we have demonstrated distinct recognition hierarchies and identified a broad conceptual framework to understand the impact of polymorphism across the KIR3DL1–HLA-I axis that will result in an improved understanding of KIR3DL1/HLA pairings in disease and transplant settings.

MATERIALS AND METHODS

Cell lines. The human HLA-Ia–deficient B-lymphoblastoid cell line 721.221 (221) was transfected with HLA-A*24:02, HLA-B*08:01, HLA-B*27:05, HLA-B*44:05, or HLA-B*57:01 via electroporation at 200 V and 975 µF (Saunders et al., 2015). 221.B58 cells were a gift from P. Parham (Stanford University, Stanford, CA). All cells were maintained in RPMI 1640 medium (Lonza) supplemented with antibiotics and 10% FBS.

Purification of NK cells and generation of KIR3DL1$^+$ NK cell clones. Human PBMCs were isolated from healthy blood donors by Ficoll/Hypaque density gradient centrifugation. Negative selection of untouched NK cells was performed using RosetteSep or EasySep Human NK Cell Enrichment kits (STEMCELL Technologies) according to the manufacturer's instructions. NKG2A$^-$KIR3DL1$^+$ (Z199$^-$DX9$^+$) cells were isolated by flow cytometry at >95% purity using a FACSAria II (BD). KIR3DL1$^+$ NK cells were cultured on irradiated feeder cells in the presence of 100 U/ml rhIL-2 (Proleukin; Chiron Corp.) and 1.5 ng/ml PHA (Gibco) and cloned by limiting dilution. Proliferating NK cell clones were analyzed for KIR3DL1 expression and the absence of NKG2A (Z270) before use in functional experiments. NK cells were maintained in RPMI 1640 supplemented with antibiotics, 10% FBS, and 100 U/ml IL-2. For donors with an unknown *KIR3DL1* allele, the expressed KIR3DL1 molecule was sequenced from extracted RNA (Saunders et al., 2015). All experiments were performed in accordance with approvals from the Human Research Ethics Committee, University of Melbourne, or the Liguria Regional Committee.

NK cell cytotoxicity. NK cell–mediated cytotoxicity was assessed in standard 4-h chromium release assays (Pende et al., 2009). In brief, effector cells were incubated with ^{51}Cr-labeled 221 transfectants at various effector/target (E:T) ratios. For masking experiments, KIR3DL1$^+$ NK cell clones were incubated with ^{51}Cr-labeled target cells, either in culture medium alone or in the presence of an anti-KIR3DL1/S1 mAb (clone Z27, IgG1) at a concentration of 10 µg/ml. Data were normalized to the maximal lysis of parental 221 target cells detected in the absence of Z27 blocking.

CD107a assay. NK cells and 221 transfectants were mixed at a 1:1 ratio and incubated for 1 h in the presence of anti-

Figure 6. **KIR3DL1*005 displays greater molecular mobility across three ligand-binding loops.** (A–F) Hydrogen–deuterium exchange of peptidic fragments from KIR3DL1. Representative *m/z* spectra of each peptidic fragment after 30 s are shown for each KIR3DL1*015 (yellow), *001 (orange), and *005 (blue) and at time 0 s (magenta). Bar graphs show the extent of deuterium exchange for each KIR3DL1 allomorph plotted at time points 0, 10, and 30 s. (A–C) Peptidic fragments derived from the KIR3DL1 D1 and D1–D2 linker. (D–F) Peptidic fragments derived from the KIR3DL1 D2. Data are from three independent experiments (each time point in triplicate). Error bars depict SEM.

CD107a-PE (BD) before the addition of monensin. The blocking antibody Y9 was added to NKG2A$^+$ NK cells before mixing with targets. After a further 3-h incubation, cells were stained with anti-NKB1-FITC (anti-KIR3DL1; BD) and anti-CD56-APC (BD), fixed in 2% paraformaldehyde, and analyzed by flow cytometry. The percentage of KIR3DL1$^+$ NK cells expressing CD107a was determined using FlowJo software (Tree Star) and normalized to maximal CD107a expression in the presence of parental 221 target cells.

Cloning and expression of KIR3DL1. The extracellular domains of KIR3DL1*001/*005/*015 (residues 1–299) were subcloned into vectors for insect cell and mammalian cell expression. For insect cell expression, the genes were subcloned into a modified baculoviral pFastBac-expression vector (Invitrogen) containing a secretion signal peptide sequence, an N-terminal hexa-histidine tag, and a C-terminal BirA tag (Stifter et al., 2014). For mammalian expression, the genes were subcloned into the pHLSec expression vector containing a secretion signal peptide sequence and an N-terminal hexa-histidine tag (Aricescu et al., 2006). Insect cell expression of KIR3DL1 was performed by baculoviral infection of BTI-TN-5B1-4 cells (Hi-5 cells; Invitrogen). Mammalian expression was performed by transient transfection of HEK293S GnTI$^-$ cells (Aricescu et al., 2006). From both cell lines, KIR3DL1 was secreted into the expression media and purified by binding to nickel Sepharose resin followed by size exclusion chromatography (S200 16/60 column; GE Healthcare). The insect cell material was used for single-antigen bead experiments but was not amenable to crystallization. The mammalian cell material was used in x-ray crystallography experiments after overnight incubation with endoglycosidase H (New England Biolabs, Inc.).

Bead assay. HLA-I recognition by KIR3DL1 allotypes was assessed through binding of KIR3DL1 tetramers to beads coated with a panel of 100 different HLA-A, -B, and -C molecules (LABScreen HLA Class I Single Antigen; One Lambda). PE-conjugated KIR3DL1 tetramer (5 μg per test) was incubated with beads for 30 min at room temperature in the dark in 300 mM of phosphate-buffered NaCl (PBS-300) with 5% fetal calf serum (AusGeneX). The beads were then washed three times in PBS-300 with 0.05% Tween 20 and resuspended in PBS-300. Binding was measured on a Luminex platform (LABScan 100; One Lambda) through identification of the individual HLA allotypes via unique bead labeling and detection of tetramer fluorescence intensity on each bead set. Normalized fluorescence values for analysis were obtained using the HLA Fusion software suite (One Lambda) that subtracted background values using the following formula:

$$(S\#N - SNC\ bead) - (BG\#N - BGNC\ bead),$$

where *S#N* is the sample-specific fluorescence value (trimmed mean) for bead *#N*, *SNC bead* is the sample-specific fluorescence value for the negative control (nude) bead, *BG#N* is the background negative control fluorescence value for bead *#N*, and *BGNC bead* is the background negative control fluorescence value for negative control bead. To obtain binding values for each HLA-I, mean fluorescence intensity (MFI) values for an isotype control (a PE-conjugated IgG) were subtracted from the raw values obtained for each experiment, and recognition was assessed as being higher than that of the tetramer to beads without conjugated HLA-I. MFI values were normalized to the highest value for each experiment and then averaged over three experiments.

Expression and purification of HLA-B*57:01. Plasmids encoding HLA-B*57:01 and β2-microglobulin were expressed separately in *Escherichia coli* and refolded in the presence of the peptide LF9. Purification of the HLA-B*57:01–LF9 complex was performed as described previously (Chessman et al., 2008).

Crystallization, data collection, structure determination, and refinement. KIR3DL1*005 and *015 expressed in mammalian HEK 293S GnTI$^-$ cells were concentrated to 12 mg/ml and combined with HLA-B*57:01–LF9 at a 1:1 molar ratio. The KIR3DL1–peptide–HLA-B*57:01 complexes were crystallized at 294K by the hanging-drop vapor-diffusion method from a solution comprising 14–18% PEG 3350, 2% Tacsimate, pH 5.0, and 0.1 M trisodium citrate, pH 5.6. Before data collection, the crystals were equilibrated in crystallization solution with 35% PEG 3350 added as a cryoprotectant and then flash-cooled in a stream of liquid nitrogen at 100K. X-ray diffraction data were collected at the MX2 beamline (Australian Synchrotron). The data were recorded on a Quantum-315 CCD detector and were integrated and scaled using MOSFLM and SCALA from the CCP4 program suite (Collaborative Computational Project, Number 4, 1994; Evans, 2006). Details of the data processing statistics are summarized in Table 1. The crystal structures were determined by molecular replacement, as implemented in PHASER (McCoy et al., 2007), with KIR3DL1*001–LF9–HLA-B*57:01 used as the search model (Protein Data Bank accession no. 3VH8 [Vivian et al., 2011]). Refinement of the models proceeded with iterative rounds of manual building in Coot (Emsley and Cowtan, 2004) and refinement in PHENIX (Adams et al., 2010). The final models comprised *N*-acetylglucosamine groups at Asn71, Asn158, and Asn252. The structures were validated with MOLPROBITY (Chen et al., 2010). Refinement statistics are summarized in Table 1. Coordinates and structure factors were deposited in the Protein Data Bank (KIR3DL1*005–HLA-B57:01–LF9, 5B38; KIR3DL1*015–HLA-B57:01–LF9, 5B39).

Peptide mapping by HPLC–tandem mass spectrometry. Peptide mapping was performed as described previously (Tsutsui et al., 2006). In brief, 5 μg of purified KIR3DL1 (in 100 μl of

100 mM Tris, pH 7.4, and 80 mM NaCl) was mixed with 95 µl of 0.5% TFA, pH 2.4. 5 µg porcine pepsin dissolved in 0.05% (vol/vol) TFA was then added over 5 min on ice. The digested sample was injected into a micropeptide trap (Grace) connected to a Everest C18 column (50 mm × 1 mm, 5 µm; Grace) and a micrOTOF mass spectrometer (Bruker). Peptidic fragments were eluted with a gradient of acetonitrile at a flow rate of 50 µl/min for tandem mass spectrometry to sequence each peptidic fragment. Peptidic fragments were identified using the Mascot search algorithm.

Hydrogen deuterium exchange analyses. Soluble KIR3DL1 (in 100 mM Tris, pH 7.4, and 50 mM NaCl) was diluted 24-fold in 100 mM Tris, pH 7.4, and 80 mM NaCl dissolved in D_2O (Cambridge Isotope Laboratories) at 25°C. The reaction was quenched at different time points by adding an equal volume of 0.5% TFA, pH 2.4, followed by rapid freezing. The first experimental time point was measured 10 s after initiation of the experiment. Frozen samples were thawed and digested with 5 µg pepsin on ice for 5 min and then injected immediately into a micropeptide trap connected to a C18 column and a micrOTOF mass spectrometer. Peptides were eluted in 12 min using a gradient of 10–45% acetonitrile at a flow rate of 50 µl/min. The micropeptide trap and C18 column were immersed in ice to minimize back exchange. To correct for any back exchange of hydrogen atoms during pepsin digestion and HPLC-MS, a fully deuterated sample was prepared by incubating 5 µg KIR3DL1 in 6 M guanidine deuterochloride, 50 mM Tris, pH 8.0, and 50 mM NaCl for 60 min at 25°C. The deuterium incorporation of each peptidic fragment, corrected for the back exchange, was calculated using the following equation: $D/N = [(m - m_{0\%})/(m_{100\%} - m)]$, where m is the mass of deuterated peptidic fragment, $m_{0\%}$ and $m_{100\%}$ are the mass of the unlabeled and fully deuterated peptidic fragments, respectively, N is the total number of exchangeable amide hydrogen atoms in each peptidic fragment, and D is the number of amide hydrogen atoms incorporated in each peptide.

ACKNOWLEDGMENTS

This research was undertaken in part on the MX2 beamline at the Australian Synchrotron, Victoria, Australia. We are grateful to Mary Diviney and Fiona Hudson at the Victorian Transplantation and Immunogenetics Service (VTIS), Australian Red Cross Blood Service, Melbourne, for training, facilities, and reagents used in the HLA-I bead assays.

This work was funded by grants from the National Health and Medical Research Council (NHMRC; 1016629, 1046685, 1062267) and the Worldwide Cancer Research organization (12-1076). This work was funded in part by the National Cancer Institute (ZIA BC010747) and the National Institutes of Health Intramural AIDS Targeted Antiviral Program. L. Moretta is supported by the Associazione Italiana per la Ricerca sul Cancro (9962). D.A. Price is supported by a Wellcome Trust Senior Investigator Award (100326/Z/12/Z). J. Rossjohn is supported by an Australia Fellowship from the NHM RC (AF50). J.P. Vivian is supported by an Australian Research Council DECRA Fellowship (130101504).

The authors declare no competing financial interests.

Submitted: 30 December 2015
Accepted: 15 March 2016

REFERENCES

Adams, P.D., P.V. Afonine, G. Bunkóczi, V.B. Chen, I.W. Davis, N. Echols, J.J. Headd, L.W. Hung, G.J. Kapral, R.W. Grosse-Kunstleve, et al. 2010. PHENIX: a comprehensive Python-based system for macromolecular structure solution. *Acta Crystallogr. D Biol. Crystallogr.* 66:213–221. http://dx.doi.org/10.1107/S0907444909052925

Aricescu, A.R., W. Lu, and E.Y. Jones. 2006. A time- and cost-efficient system for high-level protein production in mammalian cells. *Acta Crystallogr. D Biol. Crystallogr.* 62:1243–1250. http://dx.doi.org/10.1107/S0907444906029799

Borrego, F., M. Ulbrecht, E.H. Weiss, J.E. Coligan, and A.G. Brooks. 1998. Recognition of human histocompatibility leukocyte antigen (HLA)-E complexed with HLA class I signal sequence-derived peptides by CD94/NKG2 confers protection from natural killer cell-mediated lysis. *J. Exp. Med.* 187:813–818. http://dx.doi.org/10.1084/jem.187.5.813

Brooks, A.G., F. Borrego, P.E. Posch, A. Patamawenu, C.J. Scorzelli, M. Ulbrecht, E.H. Weiss, and J.E. Coligan. 1999. Specific recognition of HLA-E, but not classical, HLA class I molecules by soluble CD94/NKG2A and NK cells. *J. Immunol.* 162:305–313.

Cao, K., J. Hollenbach, X. Shi, W. Shi, M. Chopek, and M.A. Fernández-Viña. 2001. Analysis of the frequencies of HLA-A, B, and C alleles and haplotypes in the five major ethnic groups of the United States reveals high levels of diversity in these loci and contrasting distribution patterns in these populations. *Hum. Immunol.* 62:1009–1030. http://dx.doi.org/10.1016/S0198-8859(01)00298-1

Carr, W.H., M.J. Pando, and P. Parham. 2005. KIR3DL1 polymorphisms that affect NK cell inhibition by HLA-Bw4 ligand. *J. Immunol.* 175:5222–5229. http://dx.doi.org/10.4049/jimmunol.175.8.5222

Cella, M., A. Longo, G.B. Ferrara, J.L. Strominger, and M. Colonna. 1994. NK3-specific natural killer cells are selectively inhibited by Bw4-positive HLA alleles with isoleucine 80. *J. Exp. Med.* 180:1235–1242. http://dx.doi.org/10.1084/jem.180.4.1235

Cella, M., H. Nakajima, F. Facchetti, T. Hoffmann, and M. Colonna. 2000. ILT receptors at the interface between lymphoid and myeloid cells. *Curr. Top. Microbiol. Immunol.* 251:161–166.

Chen, V.B., W.B. Arendall III, J.J. Headd, D.A. Keedy, R.M. Immormino, G.J. Kapral, L.W. Murray, J.S. Richardson, and D.C. Richardson. 2010. MolProbity: all-atom structure validation for macromolecular crystallography. *Acta Crystallogr. D Biol. Crystallogr.* 66:12–21. http://dx.doi.org/10.1107/S0907444909042073

Chessman, D., L. Kostenko, T. Lethborg, A.W. Purcell, N.A. Williamson, Z. Chen, L. Kjer-Nielsen, N.A. Mifsud, B.D. Tait, R. Holdsworth, et al. 2008. Human leukocyte antigen class I-restricted activation of $CD8^+$ T cells provides the immunogenetic basis of a systemic drug hypersensitivity. *Immunity.* 28:822–832. http://dx.doi.org/10.1016/j.immuni.2008.04.020

Collaborative Computational Project, Number 4. 1994. The CCP4 suite: programs for protein crystallography. *Acta Crystallogr. D Biol. Crystallogr.* 50:760–763. http://dx.doi.org/10.1107/S0907444994003112

Cooley, S., D.J. Weisdorf, L.A. Guethlein, J.P. Klein, T. Wang, S.G. Marsh, S. Spellman, M.D. Haagenson, K. Saeturn, M. Ladner, et al. 2014. Donor killer cell Ig-like receptor B haplotypes, recipient HLA-C1, and HLA-C mismatch enhance the clinical benefit of unrelated transplantation for acute myelogenous leukemia. *J. Immunol.* 192:4592–4600. http://dx.doi.org/10.4049/jimmunol.1302517

Emsley, P., and K. Cowtan. 2004. Coot: model-building tools for molecular graphics. *Acta Crystallogr. D Biol. Crystallogr.* 60:2126–2132. http://dx.doi.org/10.1107/S0907444904019158

Evans, P. 2006. Scaling and assessment of data quality. *Acta Crystallogr. D Biol. Crystallogr.* 62:72–82. http://dx.doi.org/10.1107/S0907444905036693

Gardiner, C.M., L.A. Guethlein, H.G. Shilling, M. Pando, W.H. Carr, R. Rajalingam, C. Vilches, and P. Parham. 2001. Different NK cell surface phenotypes defined by the DX9 antibody are due to KIR3DL1 gene

polymorphism. *J. Immunol.* 166:2992–3001. http://dx.doi.org/10.4049/jimmunol.166.5.2992

Gumperz, J.E., V. Litwin, J.H. Phillips, L.L. Lanier, and P. Parham. 1995. The Bw4 public epitope of HLA-B molecules confers reactivity with natural killer cell clones that express NKB1, a putative HLA receptor. *J. Exp. Med.* 181:1133–1144. http://dx.doi.org/10.1084/jem.181.3.1133

Gumperz, J.E., L.D. Barber, N.M. Valiante, L. Percival, J.H. Phillips, L.L. Lanier, and P. Parham. 1997. Conserved and variable residues within the Bw4 motif of HLA-B make separable contributions to recognition by the NKB1 killer cell-inhibitory receptor. *J. Immunol.* 158:5237–5241.

Kuranov, A.B., I. Kötter, J.C. Henes, S.T. Abisheva, I. Steiert, F. Riewerts, K.T. Momynaliev, and C.A. Müller. 2014. Behçet's disease in HLA-B*51 negative Germans and Turks shows association with HLA-Bw4-80I. *Arthritis Res. Ther.* 16:R116. http://dx.doi.org/10.1186/ar4569

Litwin, V., J. Gumperz, P. Parham, J.H. Phillips, and L.L. Lanier. 1994. NKB1: a natural killer cell receptor involved in the recognition of polymorphic HLA-B molecules. *J. Exp. Med.* 180:537–543. http://dx.doi.org/10.1084/jem.180.2.537

Ljunggren, H.G., and K. Kärre. 1990. In search of the 'missing self': MHC molecules and NK cell recognition. *Immunol. Today.* 11:237–244. http://dx.doi.org/10.1016/0167-5699(90)90097-S

Luque, I., R. Solana, M.D. Galiani, R. González, F. García, J.A. López de Castro, and J. Peña. 1996. Threonine 80 on HLA-B27 confers protection against lysis by a group of natural killer clones. *Eur. J. Immunol.* 26:1974–1977. http://dx.doi.org/10.1002/eji.1830260845

Malnati, M.S., M. Peruzzi, K.C. Parker, W.E. Biddison, E. Ciccone, A. Moretta, and E.O. Long. 1995. Peptide specificity in the recognition of MHC class I by natural killer cell clones. *Science.* 267:1016–1018. http://dx.doi.org/10.1126/science.7863326

Marra, J., J. Greene, J. Hwang, J. Du, L. Damon, T. Martin, and J.M. Venstrom. 2015. KIR and HLA genotypes predictive of low-affinity interactions are associated with lower relapse in autologous hematopoietic cell transplantation for acute myeloid leukemia. *J. Immunol.* 194:4222–4230. http://dx.doi.org/10.4049/jimmunol.1402124

Martin, M.P., Y. Qi, X. Gao, E. Yamada, J.N. Martin, F. Pereyra, S. Colombo, E.E. Brown, W.L. Shupert, J. Phair, et al. 2007. Innate partnership of HLA-B and KIR3DL1 subtypes against HIV-1. *Nat. Genet.* 39:733–740. http://dx.doi.org/10.1038/ng2035

McCoy, A.J., R.W. Grosse-Kunstleve, P.D. Adams, M.D. Winn, L.C. Storoni, and R.J. Read. 2007. Phaser crystallographic software. *J. Appl. Cryst.* 40:658–674. http://dx.doi.org/10.1107/S0021889807021206

Mulrooney, T.J., A.C. Zhang, Y. Goldgur, J.E. Boudreau, and K.C. Hsu. 2015. KIR3DS1-specific D0 domain polymorphisms disrupt KIR3DL1 surface expression and HLA binding. *J. Immunol.* 195:1242–1250. http://dx.doi.org/10.4049/jimmunol.1500243

Norman, P.J., L. Abi-Rached, K. Gendzekhadze, D. Korbel, M. Gleimer, D. Rowley, D. Bruno, C.V. Carrington, D. Chandanayingyong, Y.H. Chang, et al. 2007. Unusual selection on the KIR3DL1/S1 natural killer cell receptor in Africans. *Nat. Genet.* 39:1092–1099. http://dx.doi.org/10.1038/ng2111

Norman, P.J., L. Abi-Rached, K. Gendzekhadze, J.A. Hammond, A.K. Moesta, D. Sharma, T. Graef, K.L. McQueen, L.A. Guethlein, C.V. Carrington, et al. 2009. Meiotic recombination generates rich diversity in NK cell receptor genes, alleles, and haplotypes. *Genome Res.* 19:757–769. http://dx.doi.org/10.1101/gr.085738.108

O'Connor, G.M., K.J. Guinan, R.T. Cunningham, D. Middleton, P. Parham, and C.M. Gardiner. 2007. Functional polymorphism of the KIR3DL1/S1 receptor on human NK cells. *J. Immunol.* 178:235–241. http://dx.doi.org/10.4049/jimmunol.178.1.235

O'Connor, G.M., J.P. Vivian, J.M. Widjaja, J.S. Bridgeman, E. Gostick, B.A. Lafont, S.K. Anderson, D.A. Price, A.G. Brooks, J. Rossjohn, and D.W. McVicar. 2014. Mutational and structural analysis of KIR3DL1 reveals a lineage-defining allotypic dimorphism that impacts both HLA and peptide sensitivity. *J. Immunol.* 192:2875–2884. http://dx.doi.org/10.4049/jimmunol.1303142

Pan, N., W. Jiang, H. Sun, F. Miao, J. Qiu, H. Jin, J. Xu, Q. Shi, W. Xie, and J. Zhang. 2011. *KIR* and *HLA* loci are associated with hepatocellular carcinoma development in patients with hepatitis B virus infection: A case-control study. *PLoS One.* 6:e25682. http://dx.doi.org/10.1371/journal.pone.0025682

Pando, M.J., C.M. Gardiner, M. Gleimer, K.L. McQueen, and P. Parham. 2003. The protein made from a common allele of KIR3DL1 (3DL1*004) is poorly expressed at cell surfaces due to substitution at positions 86 in Ig domain 0 and 182 in Ig domain 1. *J. Immunol.* 171:6640–6649. http://dx.doi.org/10.4049/jimmunol.171.12.6640

Parham, P., P.J. Norman, L. Abi-Rached, and L.A. Guethlein. 2012. Human-specific evolution of killer cell immunoglobulin-like receptor recognition of major histocompatibility complex class I molecules. *Philos. Trans. R. Soc. Lond. B Biol. Sci.* 367:800–811. http://dx.doi.org/10.1098/rstb.2011.0266

Pende, D., S. Marcenaro, M. Falco, S. Martini, M.E. Bernardo, D. Montagna, E. Romeo, C. Cognet, M. Martinetti, R. Maccario, et al. 2009. Anti-leukemia activity of alloreactive NK cells in KIR ligand-mismatched haploidentical HSCT for pediatric patients: evaluation of the functional role of activating KIR and redefinition of inhibitory KIR specificity. *Blood.* 113:3119–3129. http://dx.doi.org/10.1182/blood-2008-06-164103

Petrie, E.J., C.S. Clements, J. Lin, L.C. Sullivan, D. Johnson, T. Huyton, A. Heroux, H.L. Hoare, T. Beddoe, H.H. Reid, et al. 2008. CD94-NKG2A recognition of human leukocyte antigen (HLA)-E bound to an HLA class I leader sequence. *J. Exp. Med.* 205:725–735. http://dx.doi.org/10.1084/jem.20072525

Robinson, J., J.A. Halliwell, J.D. Hayhurst, P. Flicek, P. Parham, and S.G. Marsh. 2015. The IPD and IMGT/HLA database: allele variant databases. *Nucleic Acids Res.* 43:D423–D431. http://dx.doi.org/10.1093/nar/gku1161

Rojo, S., N. Wagtmann, and E.O. Long. 1997. Binding of a soluble p70 killer cell inhibitory receptor to HLA-B*5101: requirement for all three p70 immunoglobulin domains. *Eur. J. Immunol.* 27:568–571. http://dx.doi.org/10.1002/eji.1830270231

Sanjanwala, B., M. Draghi, P.J. Norman, L.A. Guethlein, and P. Parham. 2008. Polymorphic sites away from the Bw4 epitope that affect interaction of Bw4+ HLA-B with KIR3DL1. *J. Immunol.* 181:6293–6300. http://dx.doi.org/10.4049/jimmunol.181.9.6293

Saunders, P.M., J.P. Vivian, N. Baschuk, T. Beddoe, J. Widjaja, G.M. O'Connor, C. Hitchen, P. Pymm, D.M. Andrews, S. Gras, et al. 2015. The interaction of KIR3DL1*001 with HLA class I molecules is dependent upon molecular microarchitecture within the Bw4 epitope. *J. Immunol.* 194:781–789. http://dx.doi.org/10.4049/jimmunol.1402542

Sharma, D., K. Bastard, L.A. Guethlein, P.J. Norman, N. Yawata, M. Yawata, M. Pando, H. Thananchai, T. Dong, S. Rowland-Jones, et al. 2009. Dimorphic motifs in D0 and D1+D2 domains of killer cell Ig-like receptor 3DL1 combine to form receptors with high, moderate, and no avidity for the complex of a peptide derived from HIV and HLA-A*2402. *J. Immunol.* 183:4569–4582. http://dx.doi.org/10.4049/jimmunol.0901734

Solberg, O.D., S.J. Mack, A.K. Lancaster, R.M. Single, Y. Tsai, A. Sanchez-Mazas, and G. Thomson. 2008. Balancing selection and heterogeneity across the classical human leukocyte antigen loci: a meta-analytic review of 497 population studies. *Hum. Immunol.* 69:443–464. http://dx.doi.org/10.1016/j.humimm.2008.05.001

Stifter, S.A., J.A. Gould, N.E. Mangan, H.H. Reid, J. Rossjohn, P.J. Hertzog, and N.A. de Weerd. 2014. Purification and biological characterization of soluble, recombinant mouse IFNβ expressed in insect cells. *Protein Expr. Purif.* 94:7–14. http://dx.doi.org/10.1016/j.pep.2013.10.019

Taner, S.B., M.J. Pando, A. Roberts, J. Schellekens, S.G. Marsh, K.J. Malmberg, P. Parham, and F.M. Brodsky. 2011. Interactions of NK cell receptor KIR3DL1*004 with chaperones and conformation-specific antibody reveal a functional folded state as well as predominant intracellular

retention. *J. Immunol.* 186:62–72. http://dx.doi.org/10.4049/jimmunol.0903657

Thananchai, H., G. Gillespie, M.P. Martin, A. Bashirova, N. Yawata, M. Yawata, P. Easterbrook, D.W. McVicar, K. Maenaka, P. Parham, et al. 2007. Cutting edge: Allele-specific and peptide-dependent interactions between KIR3DL1 and HLA-A and HLA-B. *J. Immunol.* 178:33–37. http://dx.doi.org/10.4049/jimmunol.178.1.33

Tsutsui, Y., L. Liu, A. Gershenson, and P.L. Wintrode. 2006. The conformational dynamics of a metastable serpin studied by hydrogen exchange and mass spectrometry. *Biochemistry.* 45:6561–6569. http://dx.doi.org/10.1021/bi060431f

Vivian, J.P., R.C. Duncan, R. Berry, G.M. O'Connor, H.H. Reid, T. Beddoe, S. Gras, P.M. Saunders, M.A. Olshina, J.M. Widjaja, et al. 2011. Killer cell immunoglobulin-like receptor 3DL1-mediated recognition of human leukocyte antigen B. *Nature.* 479:401–405. http://dx.doi.org/10.1038/nature10517

Yawata, M., N. Yawata, M. Draghi, A.-M. Little, F. Partheniou, and P. Parham. 2006. Roles for HLA and KIR polymorphisms in natural killer cell repertoire selection and modulation of effector function. *J. Exp. Med.* 203:633–645. (published erratum appears in *J. Exp. Med.* 2006. 203:1131) http://dx.doi.org/10.1084/jem.20051884